http://informahealthcare.com/nan
ISSN: 1743-5390 (print), 1743-5404 (electronic)

Nanotoxicology

Nanotoxicology, Early Online: 1–12
 DOI: 10.3109/17435390.2014.918203

informa
healthcare

ORIGINAL ARTICLE

Identifying contact-mediated, localized toxic effects of MWCNT aggregates on epithelial monolayers: A single-cell monitoring toxicity assay

Bianca M. Rotoli[1], Rita Gatti[2],Dania Movia[3], Massimiliano G. Bianchi[4], Luisana Di Cristo[4], Ivana Fenoglio[5], Fabio Sonvico[6], Enrico Bergamaschi[4], Adriele Prina-Mello[3,7], and Ovidio Bussolati[1]

[1]Unit of General Pathology, [2]Unit of Anatomy and Histology, Department of Biomedical, Biotechnological and Translational Sciences (SBiBiT), University of Parma, Parma, Italy, [3]Centre for Research on Adaptive Nanostructures and Nanodevices (CRANN), Trinity College Dublin, Dublin, Ireland, [4]Unit of Occupational Medicine, Department of Clinical and Experimental Medicine, Parma, Italy,, [5]Interdepartmental Centre "G. Scansetti" for Studies on Asbestos and Other Toxic Particulate and Department of Inorganic Chemistry, Physical Chemistry and Material Chemistry, University of Torino, Torino, Italy, [6]Department of Pharmacy, University of Sidney, Sidney, Australia, and [7]School of Medicine, Trinity College Dublin, Dublin, Ireland

Abstract

Aggregates of multiwalled carbon nanotubes (MWCNT) impair the barrier properties of human airway cell monolayers. To resolve the mechanism of the barrier alteration, monolayers of Calu-3 human airway epithelial cells were exposed to aggregated MWCNT. At the cell-population level, trans-epithelial electrical resistance (TEER) was used as an indicator of barrier competence, caspase activity was assessed with standard biochemical assays, and cell viability was investigated by biochemical techniques and high-throughput (HTP) technique based on automated epifluorescence microscopy. At cell level, the response to MWCNT was investigated with confocal microscopy, by evaluating cell death (calcein/propidium iodide (PI)), proliferation (Ki-67), and apoptosis (caspase activity). At the cell-population level, exposure to aggregated MWCNT caused a decrease in TEER, which was not associated with a decrease in cell viability or onset of apoptosis even after an 8-d exposure. In contrast, confocal imaging demonstrated contact with MWCNT aggregates triggered cell death after 24 h of exposure. In the presence of a natural surfactant, both TEER decrease and contact-mediated toxicity were mitigated. With confocal imaging, increased proliferation and apoptosis were detected in Calu-3 cells next to the aggregates. Contact-mediated cytotoxicity was recorded in two additional cell lines (BEAS-2B and A549) derived from human airways. Similar results were confirmed by adopting two additional MWCNT preparations with different physico-chemical features. This indicates MWCNT caused localized damage to airway epithelial monolayers *in vitro* and altered the apoptotic and proliferative rate of epithelial cells in close proximity to the aggregates. These findings provide evidence on the pathway by which MWCNT aggregates impair airway barrier function, and support the use of imaging techniques as a possible regulatory-decision supporting tool to identify effects of aggregated nanomaterials not readily detected at cell population level.

Abbreviations: Calcein-AM: calcein-acetoxymethylester; PI: propidium iodide; DMEM: Dulbecco's Modified Eagle Medium; FBS: fetal bovine serum; h: hours; min: minutes; d: days; MWCNT: multiwalled carbon nanotubes; MWCNT-SA: MWCNT provided by Sigma-Aldrich cat. no. 659258; TEER: trans-epithelial electrical resistance

Keywords

Carbon nanotubes, cytotoxicity, lung epithelial barrier, proliferation, trans-epithelial electrical resistance

History

Received 29 October 2013
Revised 21 April 2014
Accepted 22 April 2014
Published online ▮▮▮

Correspondence: AdrielePrina-Mello, PhD, MSc, School of Medicine and CRANN, Institute of Molecular Medicine, Trinity Centre of Health Sciences, St. James's Street, Dublin 8, Ireland. Tel: +353 1 896 3259/ 3087. E-mail: prinamea@tcd.ie.
Enrico Bergamaschi, MD, PhD, Laboratory of Industrial Toxicology, Department of Clinical and Experimental Medicine, University of Parma, Via Gramsci, 14, 43100 Parma, Italy. Tel: +39 0521 033096. E-mail: enrico.bergamaschi@unipr.it

Introduction

Multiwalled carbon nanotubes (MWCNT) have raised great interest for their peculiar mechanical and electrical properties as reinforcing agents in novel hybrid or polymeric composites combining the beneficial properties of multiple materials. In biology, hydrogels doped with MWCNT, which mimic biological extracellular matrix (ECM), have demonstrated to provide cells with mechanical support and cues to regulate their behavior (Dong et al., 2013; Lee et al., 2009). Recent studies have investigated in depth the consequences of the interaction of

MWCNT with biological systems, highlighting severe toxic effects induced by these materials (Kayat et al., 2011; Mercer et al., 2013; Porter et al., 2013; Shvedova et al., 2013; Wang et al., 2013).

Airway epithelium represents one of the first body barriers encountered by MWCNT dispersed in the environment (Smart et al., 2006). For this reason, a wide number of studies have been investigated, *in vitro* and *in vivo*, the effect of MWCNT on the lung barrier. The concerns on the pulmonary impairment following MWCNT accumulation in the lungs and the potential systemic adverse effects of this nanomaterial on humans are indeed well documented (Shvedova et al., 2009, 2012). *In vitro*, low acute toxicity has been reported in alveolar epithelial (A549) cells, using standard biochemical methods (Pulskamp et al., 2007). However, more sensitive methods, such as colony forming efficiency assay, have shown a moderate toxicity of MWCNT (Ponti et al., 2010), and it is known that MWCNT are genotoxic for rat lung epithelial cells (Muller et al., 2008a, b). A prolonged exposure to rigid MWCNT (see ''Methods'' and ''Results'' sections for a detailed characterization) impairs the barrier function of the epithelial monolayers, lowering the trans-epithelial electrical resistance (TEER) and increasing the paracellular permeability to mannitol (Rotoli et al., 2008, 2009). Interestingly, these changes were not associated with decreased cell viability or with an altered expression of tight junction proteins, while they seemed to be related to the fibre-like properties of MWCNT (Rotoli et al., 2009). *In vivo*, rodents receiving MWCNT by intratracheal instillation or pharyngeal aspiration showed early formation of granulomas and fibrosis at deposition sites, leading to functional respiratory impairment (Kim et al., 2010; Ravichandran et al., 2009, 2010; Reddy et al., 2010). Several reports suggest a pro-allergic effect following intratracheal instillation of MWCNT in mice, with an increased production of Th2 cytokines (such as IL-4, IL-5, and IL-10) (Park et al., 2009), exacerbation of allergic airway inflammation (Inoue et al., 2009) and increased occurrence of fibrosis (Ryman-Rasmussen et al., 2009). Moreover, sub-chronic inhalation exposure of rats to MWCNT revealed early epithelial cell hyper- and/or metaplasia in the upper respiratory tract and, at high doses, a time-dependent bronchiolo-alveolar hyperplasia in the lower respiratory tract (Pauluhn, 2010).

To the best of the authors' knowledge, the mechanisms underlying the alterations of the lung barrier triggered by MWCNT *in vivo* have not been elucidated so far. Given the high tendency of MWCNT to aggregate (Kishore et al., 2009; Muller et al., 2005; Rotoli et al., 2008) and the presence of aggregates in the airway walls of exposed animals (Park et al., 2009; Pauluhn, 2009; Reddy et al., 2010), our working hypothesis is that, similar to asbestos, MWCNT aggregates might elicit peculiar toxic responses in the lungs. Due to structural similarities in terms of their ''needle-like'' shape, in combination with their high aspect ratio and low solubility, it has been hypothesized, in fact, that MWCNT may exhibit respiratory toxic properties similar to those of other fibrous materials (e.g. asbestos and nickel nanowires (Murphy et al., 2011; Poland et al., 2012), the toxicity mechanisms of which are related to the fibre pathogenicity and the frustrated phagocytosis paradigms (Donaldson et al., 2010). Indeed, numerous *in vivo* studies have already demonstrated that MWCNT, when instilled into the lungs of rodents, have the potential to cause transient inflammatory changes, granuloma formation, and fibrosis in the lung tissue (Murphy et al., 2011). Long (>20 μm), straight MWCNT have also been shown to have the potential to cause inflammation and granuloma formation in the mesothelial lining of the pleura, consistent with the pathogenic behavior of asbestos. However, information of morphological and functional events occurring in the early stages of nano-bio-interactions is still lacking. Our working strategy was, therefore, to investigate the role of MWCNT aggregates in the barrier impairment, so as to elucidate the potential mechanism of lung toxicity of this nanomaterial when present in the environment.

An *in vitro* model consisting of Calu-3 cell monolayers grown on permeable filters in a double-chamber culture system was adopted to mimic the airway epithelial barrier. Under these conditions, Calu-3 cells, which are derived from a human lung adenocarcinoma, form tight junctions, show strictly polarized secretory and transport functions, prevent the trans-epithelial passage of paracellular substrates, and participate in signal transduction (Cereijido et al., 2008; Matter & Balda 2007), thus representing an *in vitro* model of a functional epithelial barrier. For this reason, Calu-3 cells have been used to predict the behavior of the respiratory barrier *in vivo* (Sakagami, 2006) and as a model to study airway permeability to nanomaterials (Daum et al., 2009; Grainger et al., 2009; Teijeiro-Osorio et al., 2009). Monolayers of human bronchial epithelial cells (BEAS-2B) and human lung alveolar carcinoma cells (A549) were also used for comparison.

Our results demonstrate that distinctive localized toxic effects could be identified in cells in direct contact with MWCNT aggregates even when no major responses were detectable at the cell-population level. Imaging techniques are here presented as possible regulatory-decision supporting tool for nanomaterial assessment highlighting the underlying evidence of interaction between MWCNT aggregates and surrounding epithelial cells.

Methods

MWCNT materials

Commercially available multi-walled carbon nanotubes (hereafter named MWCNT-SA) used in this study as ''fibre-like'' model of nanomaterials causing respiratory toxicity (Li et al., 2007; Muller et al., 2005, 2008b; Elgrabli et al., 2008; Simon-Deckers et al., 2008), were obtained from Sigma-Aldrich (Milan, Italy, cat. no. 659258, produced through Chemical Vapor Deposition, diameter ranging between 110 and 170 nm; length ranging between 5 and 9 μm). As by manufacturer analysis, the percentage of MWCNT content was at least 90% with a residual amorphous carbon content present in the sample. The iron concentration declared by the manufacturer was less than 0.1%; however, no metal impurities were found in the preparation (see below, Results, Physico-chemical characterization of MWCNT-SA).

Two additional MWCNT preparations, NM400 and NM402, were obtained from the JRC repository of Representative Test Materials (Roebben et al., 2013) and used in this work. NM400 MWCNT have a diameter ranging between 5 and 35 nm and a length ranging between 0.7 and 3 μm, while NM402 MWCNT have a diameter ranging between 6 and 20 nm and a length ranging between 0.7 and 4 μm (Kermanizadeh et al., 2012).

Before toxicity experiments, MWCNT were heated at 220 °C for 3 h to ensure endotoxin elimination (Muller et al., 2005).

Chemicals and reagents

All reagents and chemicals used in this work, unless differently indicated, were purchased from Sigma-Aldrich (Milan, Italy). Fetal bovine serum (FBS) and culture media were purchased from EuroClone (Milan, Italy). Pluronic F127 was obtained from Invitrogen SpA (San Giuliano Milanese, Milan, Italy). The natural surfactant Curosurf®, consisting of pig lung surfactant, was kindly supplied by Chiesi Farmaceutici SpA (Parma, Italy). The

Curosurf® used in this work contained phosphatidylcholine (73% of the total phosphorus) and 1.7 mg/ml of surfactant proteins (SP-B and SP-C).

Physico-chemical characterization of MWCNT

Methods for the physico-chemical characterization of MWCNT-SA are reported in Supplementary material.

Cell culture

Calu-3 cells were routinely culturedat physiological conditions (37.5 °C, 5% CO_2, 95% humidity) in 10-cm diameter dishes in Eagle's Minimum Essential Medium (EMEM) supplemented with 1 mM sodium pyruvate, 10% FBS, streptomycin (100 µg/ml), and penicillin (100 U/ml), as previously reported (Rotoli et al., 2008). BEAS-2B and A549 cells were cultured in Dulbecco's Modified Eagle Medium (DMEM) (Euroclone, Italy), supplemented with Gln (4 mM) and 10% FBS. For the experiments, cells were seeded into culture inserts with permeable membrane filters (pore size of 0.4 µm) for Falcon 24-well-multitrays (BD Bioscience, Franklin Lakes, NJ), at a density of 75×10^3 cells/300 µl of media.

Confocal laser scanning microscopy (CLSM)

Confocal analysis was carried out with a LSM 510 Meta scan head integrated with an inverted microscope (Carl Zeiss, Jena, Germany). Samples were observed through a $40 \times (1.3\,NA)$ or a $63 \times (1.4\,NA)$ oil objectives. Image acquisition was carried out in multitrack mode, i.e. through consecutive and independent optical pathways. Vertical sections were obtained with the function Display – Cut (Expert Mode) of the LSM 510 confocal microscope software (Microscopy Systems, Hartford, CT). Reconstructions were performed from z-stacks of digital images (minimum 32 confocal sections, *z*-axis acquisition interval of 0.39 µm), processed with the Axiovision module inside 4D release 4.5 (Carl Zeiss, Jena, Germany), applying the shadow or the transparency algorithm.

Exposure to MWCNT

MWCNT were dispersed, unless otherwise stated, at a mass concentration of 1 mg/ml in sterile phosphate-buffered saline (PBS) obtaining the stock suspension. Working concentrations were obtained by serial dilutions.

MWCNT dispersions were added immediately after sonication (15 min, 3 cycles) to the growth medium at the apical side of the permeable filter on which cell monolayers were growing. The doses of MWCNT were expressed in µg/cm^2 of monolayer. The conversion of doses expressed in µg/ml into this metric depends on the ratio between culture surface and incubation volume. Thus, for cells seeded into filters of double chamber culture systems (surface 0.3 cm^2) in 225 µl of medium (apical compartment), a dose of 100 µg/ml corresponds to an average exposure of 75 µg/cm^2 of cell monolayer.

Trans-epithelial electrical resistance (TEER) measurements

Measurements of TEER of Calu-3 cells monolayers were made with an epithelial voltmeter (EVOM, World Precision Instruments Inc., Sarasota, FL) that produces an AC current. Cells were allowed to grow for 10 d into a tight monolayer (TEER > 1000 Ω cm^2) before MWCNT were added at the doses of 0, 15, 30, 45, and 75 µg/cm^2. Cells monolayers were exposed for 24 h and 8 d. In accordance with the scientific literature (Salem et al., 2009), variations in TEER were expressed as the percentage of the initial value adjusted for control cell layers according to the following equation:

$$\%\cdot\Delta_{TEER} = \frac{\text{Final TEER}_{(MWCNT-treated)}}{\text{Final TEER}_{(control)}} \times \frac{\text{Initial TEER}_{(control)}}{\text{Initial TEER}_{(MWCNT-treated)}} \times 100$$

Resazurin assay

To assess cell viability, the resazurin assay (O'Brien et al., 2000) was used. After the exposure to MWCNT (75 µg/cm^2), Calu-3 cells monolayers were incubated for 90 min with fresh, serum-free medium supplemented with 44 µM resazurin, added to both the basolateral and the apical compartments. MWCNT have been previously reported to not interfere with the resazurin assay (Rotoli et al., 2008). Fluorescence measurements at 572 nm were performed on the medium of the apical chamber transferred in a clean 96-well dish with a Wallac 1420 Victor^2 Multilabel Counter (Perkin Elmer, Waltham, MA).

Caspase activity

Cells were mechanically detached from the filter and centrifuged at $300 \times g$ for 5 min. Pellets were suspended in 500 µl of assay buffer (50 mM Hepes, 0.1% CHAPS, 10 mM EDTA, 5% glycerol, and 10 mM DTT) and vigorously vortexed. After centrifugation at $12\,000 \times g$ for 10 min at 4 °C, the protein content in the supernatant was determined with the Bio-Rad protein assay. Aliquots of 10 µg protein were distributed in each well of a 96-well plate, along with the caspase substrate Ac-DEVD-pNA (200 µM, Alexis Biochemicals, San Diego, CA). The absorbance at 405 nM was read with a microplate reader (Wallac 1420 Victor^2 Multilabel Counter, Perkin Elmer, Akron, OH) after 16 h at 37 °C. Caspase activity under each condition was expressed as the % of the value obtained for the untreated control cells after subtraction of the blank value.

Cytotoxicity analysis: live cell monolayers

Calcein/PI assay: this assay is known to not interact with MWCNT (Monteiro-Riviere et al., 2009) and it has been successfully used to determine the cytotoxic effect of carbon-based materials in previous studies (Movia et al., 2011). After exposure to MWCNT (0, 15, 30, 45, and 75 µg/cm^2) for 24 h and 8 d, the cell culture medium was replaced with fresh, complete medium containing 2.5 µM calcein–acetoxymethylester (Calcein-AM, Invitrogen, Paisley, UK) and 4 µg/ml PI. Calcein-AM is a non-fluorescent molecule that passively enters live cells where it is converted into a green fluorescent dye (calcein) by intracellular esterases. Calcein is retained by live cells until the plasma membrane is intact. PI is a red fluorescent dye that stains cells with compromised cell membrane binding to nucleic acids. Cells were incubated for 15 min at 37 °C and then washed with fresh medium. The permeable filters were then detached from the culture inserts and live specimens were imaged by an inverted LSM 510 Meta confocal microscope (Carl Zeiss, Jena, Germany) while incubated with a fresh medium in a Kit Cell Observer (Carl Zeiss, Jena, Germany), which allowed for fine temperature control, CO_2/air ratio and humidity (Gatti et al., 2008). Samples were observed through a $40 \times (1.3\,NA)$ or a $63 \times (1.4\,NA)$ oil objectives. Calcein was excited with a 488 nm laser and the emission recorded through a 505–530 nm band pass barrier filter. PI was excited with a 543 nm laser and the emission recorded through a 560 long pass barrier filter. MWCNT were imaged in reflection mode at $\lambda_{exc} = 633$ nm and are shown in

pseudo-color. Images were then processed as previously described. For quantification of PI-positive cells, six random chosen fields (approximately 0.1 mm^2) were analyzed through a series of horizontal sections.

Quantitative analysis for live/dead accounts was carried out on large areas (approximately 1 cm^2 each) of the prepared samples by HTP technique based on automated epifluorescence microscopy (Nikon TE2000, Tokyo, Japan). HTP analysis of the data was carried out by bioinformatics algorithm based on cell live/dead counting. To provide statistical sample populations, two membranes where analyzed for Calu-3 cells: Calu-3 exposed to MWCNT for 8 d and Calu-3 not exposed as a negative control. PI or Calcein staining was recorded based on their respective emission wavelengths. On an average, 400 cells were counted for each membrane. The percentage (%) of live cells was then calculated from the counting readings as described in the following equation:

$$\%\ \text{live cells} = \frac{\text{Live cells (calcein)}}{\text{Total number of cells (cell count)}} \times 100$$

Caspase activity: After exposure to MWCNT (75 $\mu g/cm^2$) for 8 d, the cell culture medium at the apical side of the cell monolayers was replaced for 1 h by fresh, complete medium supplemented with a sulforhodamine-labeled inhibitor of active caspases (CaspaTag™ Pan-Caspase in Situ Assay kit, Chemicon International, Temecula, CA). The inhibitor covalently binds to a reactive cytokine residue. Upon washing, the bound reagent is retained while the unbound reagent diffuses out of the cell, so that only cells with high caspase activity remain labeled. Negative (untreated) and positive (doxorubicin, 1 μM, 24 h) controls were included in the experimental design. The permeable filters were then detached from the culture inserts and analyzed by confocal microscopy as previously described for the calcein/PI assay. The sulforhodamine label was excited with a 543 nm laser and its emission recorded through a 560 long-pass barrier filter.

Immunofluorescence staining: fixed cell monolayers

Cell monolayers, grown on permeable filters, were rinsed in PBS and fixed with 3.7% paraformaldehyde (PFA) at room temperature for 15 min. Following staining procedures, specimens were mounted on glass slides with fluorescence mounting medium (Dako Italia SpA) and imaged by confocal microscopy (excitation at 488 nm; emission recorded through a 505–530 nm band pass barrier filter).

Proliferative activity: Actively proliferating cells were detected from the positivity to the nuclear antigen Ki-67, a protein expressed by cells in G_1, S, G_2, or M phases, but not by quiescent cells in G_0 (Scholzen & Gerdes, 2000). For this assay, cells were permeabilized with methanol at −10 °C (5 min), incubated in blocking solution (10% goat serum) at room temperature, and incubated with primary anti-Ki-67 mouse monoclonal antibody (Santa Cruz Biotechnology (Santa Cruz, CA), 1:000 + 1.5% goat serum) for 60 min. Filters were then washed in PBS and incubated with 1:400 Alexa 488 anti-mouse IgG (Invitrogen, Paisley, UK) for 45 min at 37 °C. After washing in Tween 0.1%, detached filters were mounted on a glass slide with mounting medium prior to confocal imaging.

Quantitative analysis of cell proliferation was carried out by HTP technique based on automated epifluorescence microscopy (Nikon, TE2000, Tokyo, Japan). HTP analysis of the data was carried out by bioinformatics algorithm based on nuclear counting and positive nuclear Ki-67-green fluorescent staining average intensity per cell. Two stained samples containing Calu-3 cell only (negative control) and Calu-3 exposed to MWCNT for 8 d were analyzed based on the intensity level of localized nuclear Ki-67-green fluorescent staining. The percentage (%) of proliferating cells was calculated from the following equation:

$$\%\ \text{proliferating cells} = \frac{\text{Ki} - 67 - \text{positive fluorescence}}{\text{Total cell count}} \times 100$$

The total cell count was based on the fluorescence intensity of nuclear staining (4′,6-diamidino-2-phenylindole (DAPI) staining, emission wavelength = 461 nm). On an average, 400 cells were counted for each membrane. Detailed data analysis is reported in Table 2.

Organization of F-actin filaments: After fixation, MWCNT-exposed cells were permeabilized with 0.1% Triton X-100 (10 min), incubated for 20 min at 37 °C with AlexaFluor-Phalloidin (10 U/ml, Invitrogen, Paisley, UK). After washing with PBS, detached filters were mounted on glass slides prior to confocal imaging.

Visualization of MWCNT aggregates in reflection mode

Images of MWCNT aggregates are reported in Supplementary Figure S1.

Statistical analysis

A one-way ANOVA with Tukey test was used to compare TEER values and monolayer viability under various experimental conditions. Differences were considered significant when $p < 0.05$. The analysis was performed with the Prism5™software (GraphPad Software Inc, San Diego, CA). Linear regression analyses were performed with the same software.

Results

Physico-chemical characterization of MWCNT-SA

High-resolution transmission electron microscopy (HR-TEM) images of MWCNT-SA (Sigma-Aldrich cat. no. 659258) showed a clean material composed mainly of individual tubes with lengths in order of several microns and diameters ranging from 100 nm to 200 nm (Figure 1A–C), consistently with the dimensions declared by the manufacturer. HR-TEM images did not show the presence of any iron impurities, which should be visible by TEM as black particles because of the high diffraction contrast of this metal. Dark areas were observable on the MWCNT surface (indicated by arrows in Figure 1A–C) and they were associated to synthetic defects onto the graphitic structure of the tubes.

HR-TEM results were confirmed by thermal gravimetric analysis (TGA). TGA was performed on MWCNT in air. A residual ash content of 0% (corresponding to a weight loss equal to 100%) was recorded at 900 °C (Figure 1D), demonstrating that no detectable traces of the metal catalyst used during MWCNT synthesis were present in the sample. Additionally, the absence of weight loss below 500 °C, which is attributed to the decomposition of organic groups in the carbon nanotubes material, confirmed that no organic chemical contaminants were present in the MWCNT sample. MWCNT, dispersed in the same culture medium used for cellular tests, exhibited a negative ζ potential (−12.01 ± 2.57 mV, Figure 1E) at neutral pH, in accordance with previously reported findings on carbon nanotubes (Hu et al., 2005; Movia et al., 2011; Saleh et al., 2010). Similar to what is observed with aqueous colloidal particles and what is reported in previous studies on carbon nanotubes, our results were indicative of a non-stable MWCNT dispersion in the culture medium (dispersion with ζ potential above + 30 mV or below −30 mV correspond to stable solutions) (American Society for Testing and Materials, 1985). Therefore, MWCNT incubated with the cell cultures were likely to be in the form of aggregates

COLOR Online / B&W in Print

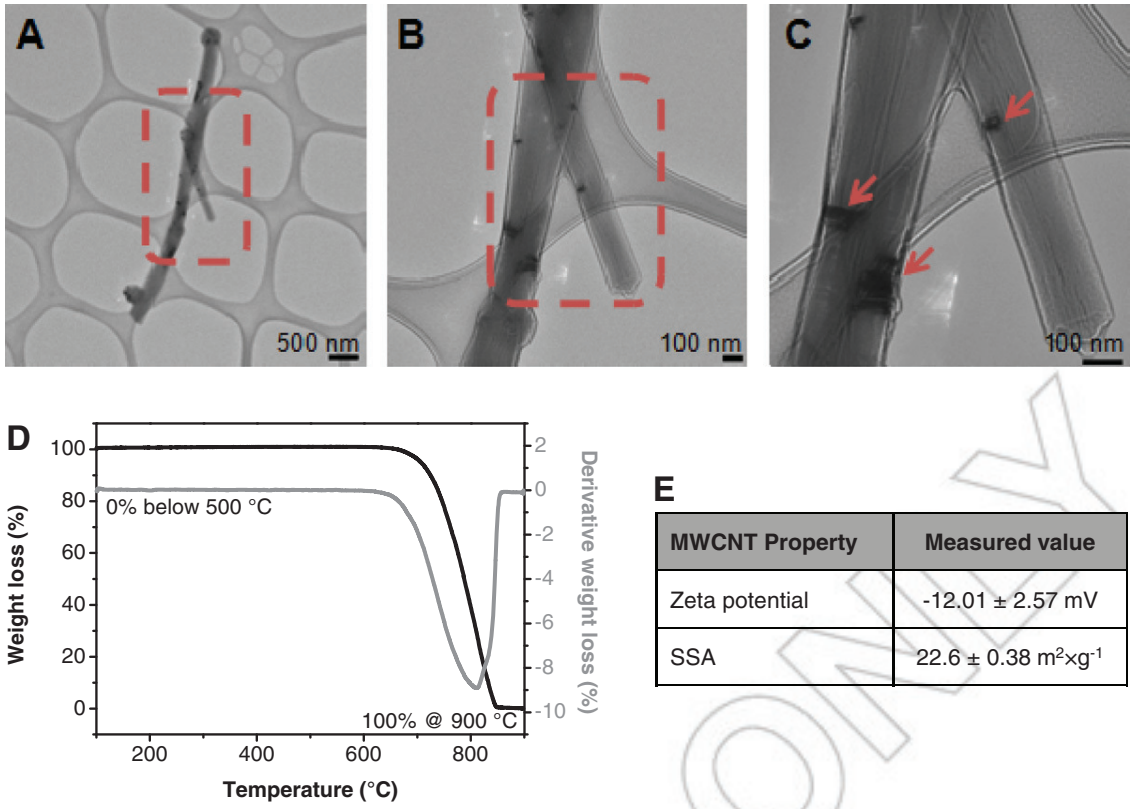

E

MWCNT Property	Measured value
Zeta potential	-12.01 ± 2.57 mV
SSA	22.6 ± 0.38 $m^2 \times g^{-1}$

Figure 1. Physico-chemical properties of MWCNT. (A–C) HR-TEM images of MWCNT on 200-mesh Cu holey carbon grids demonstrating the absence of metal impurities in the specimen. Images B and C are enlargements of the field showed in image A: red boxes highlight the areas analyzed in detail. Examples of defects in the graphitic structure of the tubes, visible as darker areas on the MWCNT surface, are indicated by arrows. (D) TGA trace of solid powder MWCNT (black line) and corresponding first derivative (grey line). The weight losses % at 500 °C and 810 °C, attributed to the decomposition of the organic groups and of the graphitic skeleton, respectively, are reported. All the experiments have been run in air atmosphere with a temperature rate of 10 °C/min. (E) Table showing zeta potential values for MWCNT dispersed in the cell medium and specific surface area (SSA) values for MWCNT dry powder.

when suspended in the culture medium. Cell monolayers tested in this study were, therefore, exposed to MWCNT aggregates, which ranged from less than 20 µm of diameter to more than 80 µm (Figure S1). Such aggregates were persistent for several days.

Finally, the specific surface area (SSA) of the MWCNT-SA sample was $22.6 \pm 0.38\ m^2\ g^{-1}$ (Figure 1E).

Analyses in live cell monolayers

TEER measurements and resazurin assay were carried out on Calu-3 cell monolayers to identify the responses of these cell cultures following exposure to MWCNT-SA (75 µg/cm^2). As demonstrated by ζ potential measurements (Figure 1E) and by confocal microscopy (Figure S1), Calu-3 cell monolayers were exposed to MWCNT in the form of aggregates.

TEER measurements showed that when Calu-3 cell monolayers were incubated with MWCNT-SA, a significant decrease in TEER was detectable (Figure 2A). A similar response was detected when Calu-3 cells were exposed to two other MWCNT preparations obtained from the JRC repository of representative test materials, NM-400 and NM-402. Calu-3 cell monolayer integrity was biochemically assessed by resazurin assay. After the exposure to MWCNT, no significant alteration of the monolayer was detectable by this assay with all the materials tested (Figure 2B). Consistently, no increase in caspase activity was detected in cell lysates of MWCNT-treated monolayers (Figure 2C).

Automated epifluorescence microscopy analysis of cell monolayers stained with calcein/propidium iodide confirmed the resazurin measurements, showing no significant changes in cell viability when Calu-3 cell monolayers were exposed to MWCNT-SA (Table 1).

The relationship between MWCNT aggregation and TEER decrease was investigated in the experiment recounted in Figure 3. In this experiment, natural and synthetic surfactants were used to delay MWCNT-SA aggregation (Figure 3A–C). The decrease in TEER, already detectable after 3 d of exposure to aggregated MWCNT (Figure 3D), was no longer observable after exposure to MWCNT-SA dispersed in the presence of the natural surfactant Curosurf® (0.8 mg/ml). Interestingly, no significant TEER changes were detected also when the natural surfactant was used alone. The decrease in TEER induced by MWCNT-SA was instead comparable in the absence or in the presence of the synthetic surfactant Pluronic (1 mg/ml), which, however, produced a significant TEER decrease even when added alone. Viability measurements (Figure 3E) performed in the same monolayers used for the TEER determinations indicated that no significant decrease in viability was detected under any of the conditions tested.

To investigate the mechanisms underlying the discrepancy between TEER measurements and cell viability assay in MWCNT-treated monolayers, we investigated the response of Calu-3 cells by confocal microscopy.

Calcein/PI assay: Untreated Calu-3 cell monolayers accumulated calcein rather homogeneously, while few or no cells were propidium positive (Figure 4A). These findings were confirmed by analysis of vertical sections (Figure 4B) and three-dimensional reconstructions (Figure 4C), which showed that the untreated

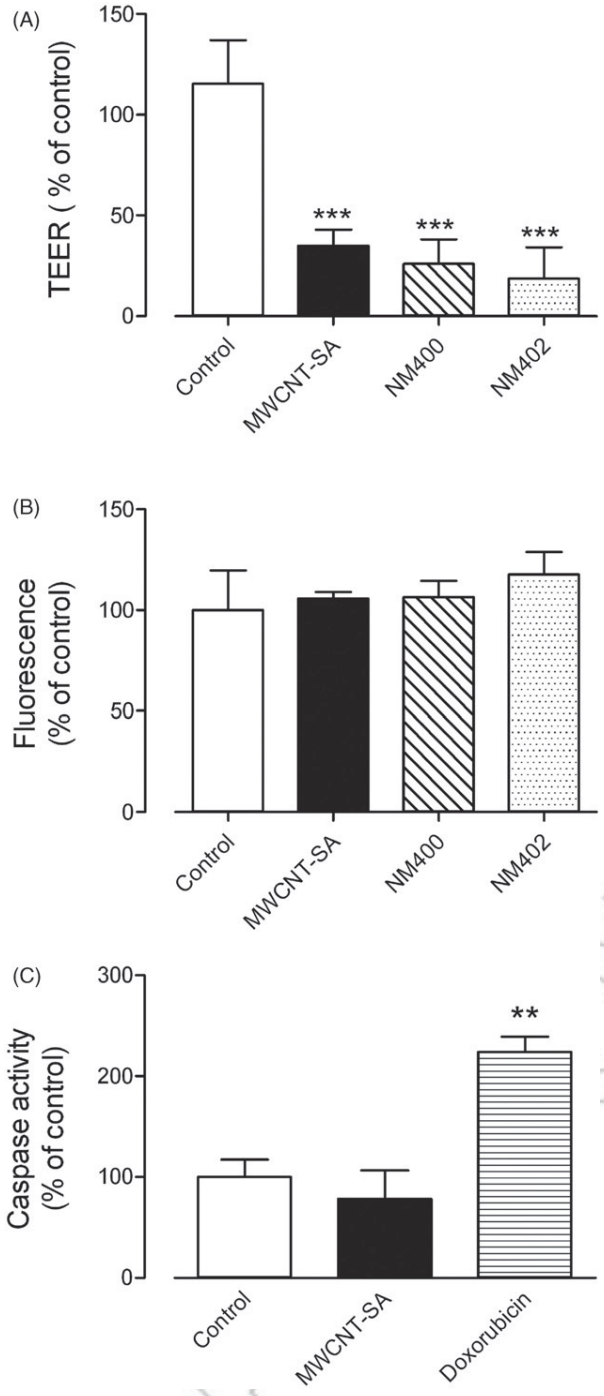

Figure 2. Determination of TEER, cell viability, and caspase activity in MWCNT-treated Calu-3 cell monolayer. Cells were incubated with the indicated materials at a dose 75 μg/cm^2. After 8 d, (A) TEER, (B) cell viability (assessed by resazurin biochemical assay), and (C) caspase activity (assessed in cell lysates) were determined. For (A) and (B), three MWCNT preparations (MWCNT-SA, NM400, and NM402) were used. For (C), only MWCNT-SA were used, while doxorubicin (1 μM, 1 d) was the positive control. Data are means ($n_{test} = 4$) ± S.D. $^{**}p < 0.01$, $^{***}p < 0.001$, versus control, untreated cultures.

Calu-3 cell monolayers were planar and intact. Propidium-positive (i.e. dead) cells appeared in Calu-3 cell monolayers exposed to MWCNT-SA for 24 h (Figure 4D). However, the distribution of dead cells was not uniform throughout the cell population because propidium-positivity was detected mainly in the close proximity of MWCNT-SA aggregates. The vertical section at 24 h of exposure (Figure 4E), taken in correspondence to the largest aggregates, also confirmed that the injury was restricted to cells in direct contact with the MWCNT-SA aggregate (arrows), while the remaining portion of the monolayer preserved its viability. Interestingly, there was no evidence of live cells present at top surface of the aggregates (imaged in reflection mode and showed in grey as pseudo-color). The top surface resulted to be completely cell-free, as demonstrated in both the vertical section and the 3D reconstruction images (Figure 4F). On the contrary, after 8 d of exposure to MWCNT-SA, confocal analysis showed that the tangles were almost covered by a monolayer of cells (Figure 4G, base of the aggregate; Figure 4H, aggregate top). The vertical section (Figure 4I) and the 3D reconstruction (Figure 4L) images evidenced that the majority of cells lying on the top of the aggregates were dead, with a minority of viable cells stained with green calcein (shown in Figure 4H by arrowheads). Notably, since propidium-positive cells were detected around the aggregates of smaller sizes than those shown in Figure 4 (Supplementary Figure S2), no definite threshold size of aggregates could be determined for contact-mediated cytotoxicity.

Contact-mediated cytotoxicity was also found in monolayers treated with the NM400 and NM402 MWCNT; also in this case, propidium-positive cells were detectable in close contact with the aggregates (Supplementary Figure S3).

In addition, the contact-mediated cytotoxicity was also observed in two additional airway epithelial cell lines, BEAS-2B and A549 treated with MWCNT-SA (Supplementary Figure S4).

Finally, the quantitative relationship between MWCNT dose and cytotoxicity was determined by quantifying the number of propidium-positive cells. For the concentrations range adopted (0, 15, 30, 45, and 75 μg/cm^2), a significant linear relationship existed between the MWCNT mass concentration and the percentage of dead cells after 8 d exposure (Figure 5A). This result was in agreement with the TEER data which evidenced a significant linear dose–effect relationship between the change in resistance of the Calu-3 cell monolayer and the MWCNT dose (Figure 5B).

Caspase activity: Confocal microscopy analysis showed that after 8 d of exposure to MWCNT-SA, caspase activity increased in several cells growing on the top of the aggregate (Figure 6A and B), whereas no caspase fluorescence was observed in untreated monolayers (Figure 6C). When co-stained with calcein, caspase-negative cells located at the top of the MWCNT aggregates showed calcein positivity (Figure 6A and B), exhibiting a granular intracellular distribution of the dye (arrowheads). This distribution differed from the intracellular distribution exhibited by untreated cells (Figure 6C), which were completely filled with calcein, with some areas of enhanced positivity. Positive control was taken as a Calu-3 cell monolayer treated with pro-apoptotic drug doxorubicin (1 μM) for 24 h (Figure 6D). Doxorubicin-treated monolayers exhibited widespread caspase activity similar to MWCNT-treated cultures, with several caspase-positive cells and calcein-positive cells characterized by the granular staining pattern.

Analyses in fixed cell monolayers

Cell proliferation: The positivity to the nuclear Ki-67 antigen was used to evaluate the proliferative behavior of Calu-3 cell monolayers incubated for 8 d in the absence or in the presence of MWCNT-SA. This assay has been widely adopted in the scientific literature to detect actively cycling cells in normal and tumor tissues (Scholzen & Gerdes, 2000). Although several isolated Ki-67-positive cells were detectable in the untreated

Table 1. High throughput screening (HTS) analysis of cell population monolayers. Quantitative analysis of cell viability (calcein/propidium iodide assay) based on 400 cells per measurement.

Calcein/propidium iodide assay					
Sample	Measurement	Number of calcein-positive cells	Number of propidium iodide-positive cells	% of live cells	Average (± standard deviation)
Untreated	1	212	188	53.00	49.83 (± 3.39)
	2	201	192	50.25	
	3	185	208	46.25	
MWCNT-treated	1	195	205	48.75	48.92 (± 1.76)
	2	189	210	47.25	
	3	203	197	50.75	

COLOR Online / B&W in Print

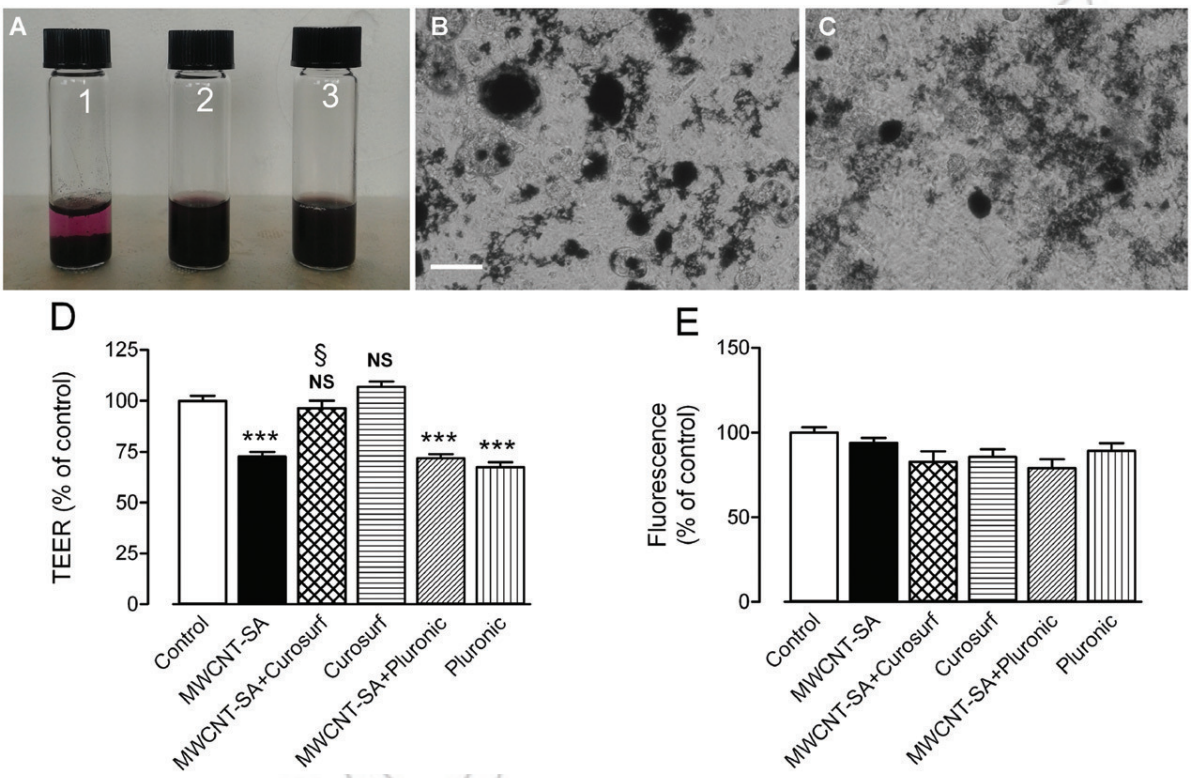

Figure 3. Effect of natural surfactant on MWCNT aggregates and on MWCNT-induced TEER decrease. (A) MWCNT-SA (1 mg/ml) were suspended in non-supplemented culture medium (EMEM, 1) or in medium supplemented with pluronic F127 (10 mg/ml, 2) or Curosurf® (8 mg/ml, 3), and the suspension was sonicated for 30 min. The image was taken 60 min after sonication. (B, C) MWCNT (75 μg/cm^2) were added to Calu-3 monolayers in the absence (B) or in the presence (C) of Curosurf® (0.8 mg/ml). Images were taken after 3 d (bar = 50 μm). (D and E) Confluent Calu-3 monolayers were incubated in normal culture medium or in culture medium supplemented with the natural surfactant Curosurf® (0.8 mg/ml) or with pluronic F127 (1 mg/ml). The incubation was performed in the absence or in the presence of MWCNT (75 μg/cm^2). After 3 d, TEER (D) and cell viability (E) (resazurin method) were measured in the same monolayers. Data are shown as average ($n_{test} = 4$) ± S.D. As a negative control, cells were incubated without either surfactants or MWCNT. (D) ***$p < 0.001$ versus control; NS, not significant versus control; §$p < 0.05$ versus cells exposed to MWCNT without surfactants.

Calu-3 cell monolayers (due to their origin from a neoplastic population with high basal proliferative activity), an increased presence of cells in active proliferation was detectable in proximity and around MWCNT aggregates (Figure 7).

Quantitative cell population level assessed by HTP did not show any difference between exposed and untreated sample, as shown in Table 2.

Discussion

This study aimed to investigate the lung toxicity properties of MWCNT in their aggregate form when coming into direct contact with cells. An imaging approach that identifies, at the cell level, contact-mediated cytotoxic effects were developed, thus overcoming the limitations imposed by current automated epifluorescent microscopy or HTP techniques and standard biochemical techniques. Here, we argue from pre-existing evidence on carbon nanotubes (Donaldson et al., 2006; Mutlu et al., 2010) and asbestos (Donaldson et al., 2010), as well as from our own experimental results, that aggregates of MWCNT are endowed with peculiar toxic properties, such as the ability to decrease TEER. Indeed, when MWCNT aggregation tendency was decreased with a natural surfactant, TEER decrease was prevented, indicating that it was attributable to aggregates rather than dispersed MWCNT. In addition, several findings (Carrero-Sanchez et al., 2006; Maynard et al., 2004) support our assumption that the possibility of being exposed to single MWCNT is low, due to their tendency to aggregate into bundles. While most

COLOR Online / B&W in Print

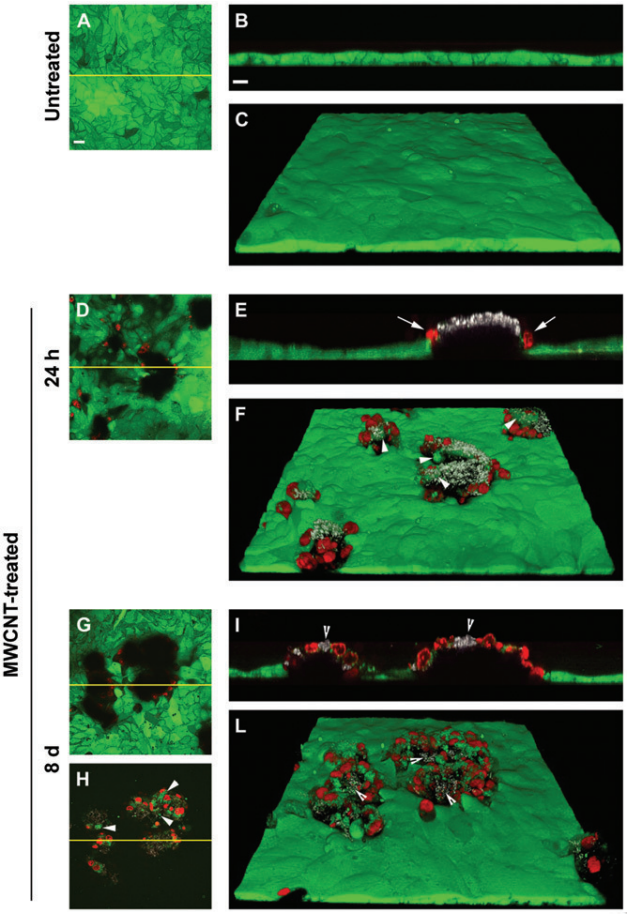

Figure 4. Confocal analysis of Calu-3 cell monolayers treated with MWCNT. Confluent monolayers of Calu-3 cells were incubated in the absence (A–C) or in the presence of MWCNT-SA (75 μg/cm^2) for 24 h (D–F) or 8 d (G–L). Live cells are shown in green (calcein), while dead cells are visualized in red (propidium iodide, PI) and aggregate free surface, visualized from the reflected light, in grey (see Supplementary Figure S1). (A, D, G, and H) Single horizontal confocal sections taken at the level of the monolayer (A, D, G) or at the top of the MWCNT aggregate (H). (B, E, and I) Vertical sections taken on the plan marked by the line shown in panels A, D, and G, respectively. (C, F, and L) Three-dimensional reconstructions of z-stack confocal images. Scale bar: 20 μm. The experiment was repeated five times with comparable results.

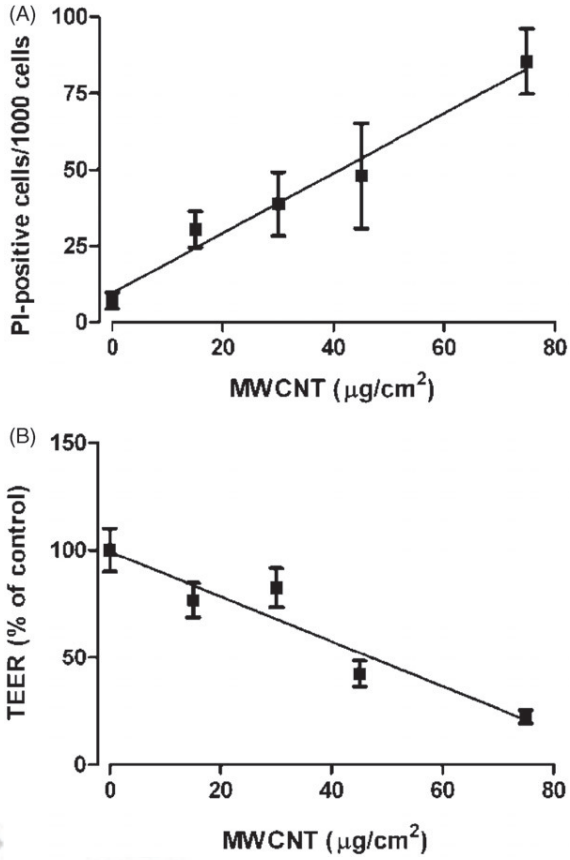

Figure 5. Dose dependency of MWCNT-induced changes in TEER and cell viability. Confluent monolayers of Calu-3 cells were incubated in the absence or in the presence of increasing doses of MWCNT-SA (15–75 μg/cm^2). After 8 d, TEER was measured (B) and monolayers visualized at confocal microscope (Figure 4) and propidium-positive cells counted (see ''Methods'' section). Data are shown as (A) mean values ($n_{test} = 4$) ± S.D. and as (B) mean TEER changes (% of control, $n_{test} = 4$) ± S.D. Straight lines represent the best-fit linear regressions.

Q5

of the data presented here were obtained with thick-diameter type, needle-like MWCNT of commercial origin (MWCNT-SA), the main findings were confirmed with two ''tangle-type'' MWCNT preparations, obtained from the JRC repository of representative test materials (Roebben et al., 2013), which are much thinner (Kermanizadeh et al., 2012) but nonetheless also form aggregates as shown in Figure S3. The importance of aggregation for the pulmonary toxicity was also proposed for single-walled carbon nanotubes (SWCNT), leading to the speculation that the aggregation of these materials, rather than their large aspect ratio accounted for the toxic effects (Mutlu et al., 2010). In particular, foci of granulomatous lesions and collagen deposition were associated with dense particle-like SWCNT agglomerates (Murray et al., 2012).

The results presented in this study show that aggregated MWCNT hinder the barrier properties of airway cells, as demonstrated by a dose-dependent decrease in TEER. Although no changes in cell viability are detected by different biochemical assays at the cell population level, confocal microscopy on living monolayers showed a distinguishable difference. In particular, confocal microscopy analysis demonstrated that the viability of cells adherent to MWCNT aggregates was severely affected, as indicated by the positivity of these cells to PI. Propidium-positive cells were already detectable after a 24 h contact with MWCNT aggregates, indicating that short-term exposure times were sufficient to induce cell death and localized cell monolayer damage. Interestingly, cell monolayers impairment was dose dependent and correlated well with the TEER changes. The dose–effect relationship shown in Figure 5(A) indicates that propidium-positive cells correspond to approximately 8% of the total cell population at the maximal mass concentration of MWCNT tested (75 μg/cm^2). This low percentage may well explain why MWCNT-induced cytotoxicity is not detected by conventional assays at whole cell population level. Additionally, these results are in agreement with the low cytotoxicity of MWCNT reported on epithelial models *in vitro* (Pulskamp et al., 2007) and with the transient inflammatory changes detected in the lungs *in vivo* (Park et al., 2009). Finally, the absence of a widespread damage to the cell monolayer is hardly compatible with the potential sequestration of essential components from the medium by adsorption onto MWCNT surface, a mechanism proposed to account for MWCNT cytotoxicity (Casey et al., 2008). In contrast, HR-TEM and TGA analyses (Figure 1A–C and D, respectively) ruled out that MWCNT cause cell damage through the diffusion in the medium of toxic factors, such as possible

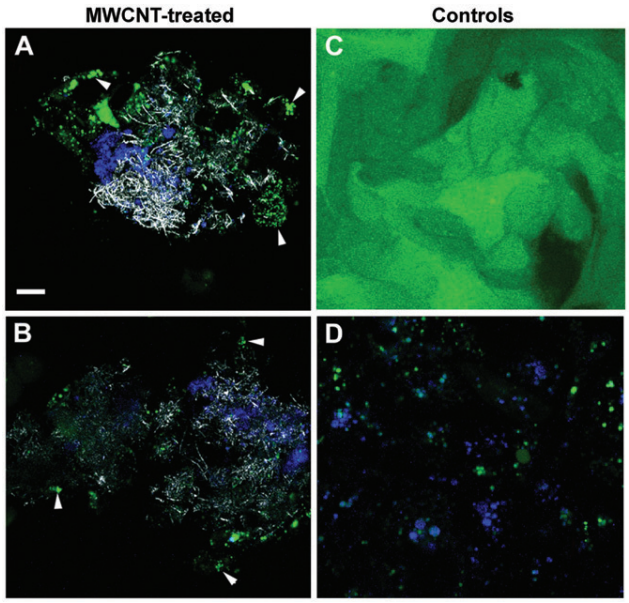

Figure 6. Caspase-positivity in MWCNT-treated Calu-3 monolayers. Figure reports representative confocal images of Calu-3 cell monolayers treated with MWCNT-SA (A and B) (75 µg/cm^2, 8 d); untreated (C); or treated for 1 d with 1 µM doxorubicin, used as a positive control for apoptosis (D). Monolayers were stained with calcein-AM and with sulforhodamine-labeled caspase-inhibitor (for caspase activity). (A and B) Cells adherent to MWCNT aggregates showed high caspase activity. Single horizontal sections, taken at the top of two MWCNT aggregates, are shown. (C) Representative field of an untreated Calu-3 cell monolayer. (D) Representative field of a caspase-positive Calu-3 cell population. Caspase signal is rendered in a blue scale, while calcein is in green and MWCNT surface is in grey. Scale bar: 10 µM.

metal or organic contaminants, which were not detected in the MWCNT-SA preparation.

The visualization of F-actin filaments constituting the cell cytoskeleton (Figure S5) demonstrates that Calu-3 cells react to the presence of MWCNT aggregates changing their shape and cytoskeletal organization. Thus, similarly to what observed for SWCNT aggregates (Worle-Knirsch et al., 2006), Calu-3 cells adhered actively to MWCNT tangles, as the first step in a colonization process. A direct interaction between actin cytoskeleton and SWCNT has been also recently described (Holt et al., 2010). However, in that case, SWCNT were dispersed and aggregates eliminated before cell treatment. In the experiment shown in Figure S5, no dispersing agent was utilized making, therefore, unlikely a direct interaction between the actin and the nanomaterial. Conversely, it is likely that epithelial cells reorganize their cytoskeleton to allow an active and close adherence to the nanomaterial. It is known that the characteristics of the adhesion surfaces have considerable consequences on the cell shape and, hence, on the cell fate (Vogel & Sheetz, 2006, 2009). MWCNT surface is highly irregular, as clearly shown by the confocal images in reflection mode (Figures 4 and S1), and may not allow firm focal adhesions by the epithelial cells (Cui et al., 2005; Lu et al., 2008). In addition, epithelial cells are more sensitive than other cell types to *anoikis*, a form of apoptosis promoted by absent or wrong signals from membrane adhesion complexes (Gilmore, 2005). Since the death process triggered by MWCNT aggregates seems asynchronous and involves individually caspase-positive cells, we suggest that *anoikis*-mediated apoptosis is a likely mechanism of the localized cytotoxicity of MWCNT aggregates, although further studies are needed to confirm this form of cell death. However, as in the case of cell

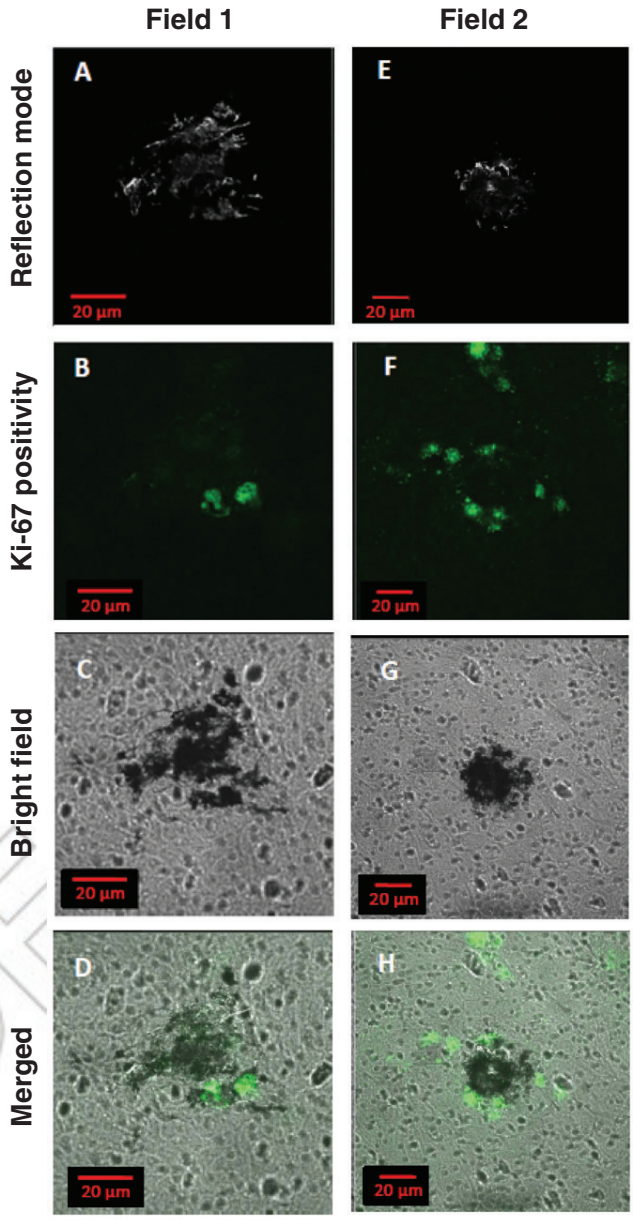

Figure 7. Confocal microscopy images of Calu-3 cell monolayers treated with MWCNT-SA (75 µg/cm^2, 8 d) and stained for Ki-67 positivity. Two representative fields (A–D and E–H) are shown. (A and E) Reflection mode showing the surface of MWCNT aggregates in grey scale. (B and F) Ki-67 positivity (green scale): actively proliferating Calu-3 cells are visible in close proximity to MWCNT aggregates. (C and G) Bright field images: MWCNT aggregates appear as black masses. (D and H) Merged images of (A. B, and C) and (E, F, and G), respectively. Scale bars: 20 µm.

viability, conventional assays of caspase activity at whole cell population level did not detect significant apoptotic changes (Figure 2C). Singularly localized apoptotic death would also be consistent with the relatively small inflammatory response associated with exposure to MWCNT found *in vivo* (Ma-Hock et al., 2009; Park et al., 2009). Apoptosis occurrence in epithelial monolayers exposed to nanomaterials has been also described in Caco-2 cells treated with polystyrene nanoparticles (Thubagere & Reinhard, 2010). However, in that work, cell death was triggered by oxidative stress; in contrast, no induction of the *Hmox1* gene was detected in MWCNT-treated Calu-3 cells, thus suggesting that no widespread oxidative stress occurs in our model (data not shown).

Table 2. High throughput screening (HTS) analysis of cell population monolayers.

Cell proliferation assay					
Sample	Measurement	Number of Ki67-positive cells	Total cell count	% of live cells	Average (± standard deviation)
Untreated	1	0.50	1.00	50.25	49.25 (± 4.34)
	2	0.44	1.00	44.50	
	3	0.53	1.00	53.00	
MWCNT-treated	1	0.49	1.00	49.50	49.00 (± 2.78)
	2	0.46	1.00	46.00	
	3	0.51	1.00	51.50	

Quantitative analysis of cell proliferation (Ki-67 assay) based on 400 cells per measurement.

In our *in vitro* model, proliferating cells were detected at high frequency in proximity of MWCNT aggregates, as evidenced by the Ki-67 positivity (Figure 7). It is tempting to attribute this behavior to the proliferative drift due to the MWCNT-induced cell death and the consequent loss of contact inhibition in the monolayer. Intriguingly, also the exposure of airway epithelium to MWCNT *in vivo* is associated with an hyperproliferative behavior, consisting in areas of epithelial hyperplasia (Ma-Hock et al., 2009) or ''thickening of epithelial cell layers'' (Pauluhn, 2010), detected in close proximity of nanomaterial aggregates.

Conclusions

This study shows that when human airway epithelial cells are exposed to MWCNT aggregates, distinctive, localized cytotoxic effects are detectable only when adopting an advanced imaging approach. Our results not only support previous data showing the potential for MWCNTs aggregates to induce lung toxicity at low doses but also incorporate methodological tools for advanced imaging of MWCNT–cell interaction. The approach described in this work represents, therefore, a first step in generating a set of suitable methodologies to exploit mechanistic studies supporting regulatory risk assessments. Moreover, this could be applied to the assessment of other toxicologically relevant parameters, such as protein translocation, changes at organelle levels, and dynamics of membrane components.

Acknowledgements

The authors would like to thank Prof. Petronini (University of Parma) for the supply of BEAS-2B and A549 cell lines. We would also like to thank Chiesi Farmaceutici SpA, Parma, Italy, for the kind donation of the natural surfactant Curosurf®.

Declaration of interest

The authors declare that they have no competing interests. This work was supported by EU FP7 Sanowork (Ref. 280716) and Marina (Ref. 263215) to E. B. D. M. was partially supported by EU FP7 NANoREG project (Ref. 310584), whereas A. P. M. was partially supported by the EU FP7 project NAMDIATREAM (Ref. 246479). M. G. B. is supported by a research scholarship of the University of Parma Medical School.

Authors' contributions

O. B., E. B., and A. P. M. conceived and designed the study, participated in its coordination, drafted the manuscript, and critically reviewed the final version of the manuscript. B. M. R. participated in the design of the study, carried out cell viability, and TEER measurements and critically reviewed the results. R. G. carried out confocal studies and critically reviewed the results. M. G. B. and L. D. C. cooperated in the confocal observations. I. F. and F. S. carried out part of the characterization experiments and critically evaluated the results. D. M. and A. P. M. carried out HR-TEM, TGA. and HTS experiments and actively reviewed the manuscript. All authors read and approved the final manuscript. B. M. R., R. G., and D. M. equally contributed to this work.

References

American Society for Testing and Materials. 1985. Zeta potential of colloids in water and waste water. ASTM Standard D 4187–82.

Carrero-Sanchez JC, Elias AL, Mancilla R, Arrellin G, Terrones H, Laclette JP, Terrones M. 2006. Biocompatibility and toxicological studies of carbon nanotubes doped with nitrogen. Nano Lett 6: 1609–16.

Casey A, Herzog E, Lyng FM, Byrne HJ, Chambers G, Davoren M. 2008. Single walled carbon nanotubes induce indirect cytotoxicity by medium depletion in A549 lung cells. Toxicol Lett 179: 78–84.

Cereijido M, Contreras RG, Shoshani L, Flores-Benitez D, Larre I. 2008. Tight junction and polarity interaction in the transporting epithelial phenotype. Biochim Biophys Acta 1778:770–93.

Cui D, Tian F, Ozkan CS, Wang M, Gao H. 2005. Effect of single wall carbon nanotubes on human HEK293 cells. Toxicol Lett 155: 73–85.

Daum N, Neumeyer A, Wahl B, Bur M, Lehr CM. 2009. *In vitro* systems for studying epithelial transport of macromolecules. Methods Mol Biol 480:151–64.

Donaldson K, Aitken R, Tran L, Stone V, Duffin R, Forrest G, Alexander A. 2006. Carbon nanotubes: a review of their properties in relation to pulmonary toxicology and workplace safety. Toxicol Sci 92:5–22.

Donaldson K, Murphy FA, Duffin R, Poland CA. 2010. Asbestos, carbon nanotubes and the pleural mesothelium: a review of the hypothesis regarding the role of long fibre retention in the parietal pleura, inflammation and mesothelioma. Part Fibre Toxicol 7:5.

Dong C, Kashon ML, Lowry D, Dordick JS, Reynolds SH, Rojanasakul Y, et al. 2013. Exposure to carbon nanotubes leads to changes in the cellular biomechanics. Adv Healthc Mater 2:945–51.

Elgrabli D, Abella-Gallart S, Robidel F, Rogerieux F, Boczkowski J, Lacroix G. 2008. Induction of apoptosis and absence of inflammation in rat lung after intratracheal instillation of multiwalled carbon nanotubes. Toxicology 253:131–6.

Gatti R, Orlandini G, Uggeri J, Belletti S, Galli C, Raspanti M, et al. 2008. Analysis of living cells grown on different titanium surfaces by time-lapse confocal microscopy. Micron 39:137–43.

Gilmore AP. 2005. Anoikis. Cell Death Differ 12:1473–7.

Grainger CI, Greenwell LL, Martin GP, Forbes B. 2009. The permeability of large molecular weight solutes following particle delivery to air-interfaced cells that model the respiratory mucosa. Eur J Pharm Biopharm 71:318–24.

Holt BD, Short PA, Rape AD, Wang YL, Islam MF, Dahl KN. 2010. Carbon nanotubes reorganize actin structures in cells and ex vivo. ACS Nano 4:4872–8.

Hu H, Yu AP, Kim E, Zhao B, Itkis ME, Bekyarova E, Haddon RC. 2005. Influence of the zeta potential on the dispersability and purification of single-walled carbon nanotubes. J Phys Chem B 109: 11520–4.

Inoue K, Koike E, Yanagisawa R, Hirano S, Nishikawa M, Takano H. 2009. Effects of multi-walled carbon nanotubes on a murine allergic airway inflammation model. Toxicol Appl Pharmacol 237:306–16.

Kayat J, Gajbhiye V, Tekade RK, Jain NK. 2011. Pulmonary toxicity of carbon nanotubes: a systematic report. Nanomedicine 7:40–9.

Kermanizadeh A, Gaiser BK, Hutchison GR, Stone V. 2012. An *in vitro* liver model – assessing oxidative stress and genotoxicity following exposure of hepatocytes to a panel of engineered nanomaterials. Part Fibre Toxicol 9:28.

Kim JE, Lim HT, Minai-Tehrani A, et al. 2010. Toxicity and clearance of intratracheally administered multiwalled carbon nanotubes from murine lung. J Toxicol Environ Health A 73:1530–43.

Kishore AS, Surekha P, Murthy PB. 2009. Assessment of the dermal and ocular irritation potential of multi-walled carbon nanotubes by using *in vitro* and *in vivo* methods. Toxicol Lett 191: 268–74.

Lee CK, Shin SR, Mun JY, et al. 2009. Tough supersoft sponge fibers with tunable stiffness from a DNA self-assembly technique. Angew Chem, Int Ed 48:5116–20.

Li JG, Li WX, Xu JY, Cai XQ, Liu RL, Li YJ, Zhao QF, Li QN. 2007. Comparative study of pathological lesions induced by multiwalled carbon nanotubes in lungs of mice by intratracheal instillation and inhalation. Environ Toxicol 22:415–21.

Lu J, Rao MP, MacDonald NC, Khang D, Webster TJ. 2008. Improved endothelial cell adhesion and proliferation on patterned titanium surfaces with rationally designed, micrometer to nanometer features. Acta Biomater 4:192–201.

Ma-Hock L, Treumann S, Strauss V, et al. 2009. Inhalation toxicity of multiwall carbon nanotubes in rats exposed for 3 months. Toxicol Sci 112:468–81.

Matter K, Balda MS. 2007. Epithelial tight junctions, gene expression and nucleo-junctional interplay. J Cell Sci 120:1505–11.

Maynard AD, Baron PA, Foley M, Shvedova AA, Kisin ER, Castranova V. 2004. Exposure to carbon nanotube material: aerosol release during the handling of unrefined single-walled carbon nanotube material. J Toxicol Environ Health A 67:87–107.

Mercer RR, Scabilloni JF, Hubbs AF, et al. 2013. Distribution and fibrotic response following inhalation exposure to multi-walled carbon nanotubes. Part Fibre Toxicol 10:33.

Monteiro-Riviere NA, Inman AO, Zhang LW. 2009. Limitations and relative utility of screening assays to assess engineered nanoparticle toxicity in a human cell line. Toxicol Appl Pharmacol 234:222–35.

Movia D, Prina-Mello A, Bazou D, Volkov Y, Giordani S. 2011. Screening the cytotoxicity of single-walled carbon nanotubes using Novel 3D tissue-mimetic models. Acs Nano 5:9278–90.

Muller J, Decordier I, Hoet PH, Lombaert N, Thomassen L, Huaux F, et al. 2008a. Clastogenic and aneugenic effects of multi-wall carbon nanotubes in epithelial cells. Carcinogenesis 29:427–33.

Muller J, Huaux F, Fonseca A, et al. 2008b. Structural defects play a major role in the acute lung toxicity of multiwall carbon nanotubes: toxicological aspects. Chem Res Toxicol 21: 1698–705.

Muller J, Huaux F, Moreau N, et al. 2005. Respiratory toxicity of multi-wall carbon nanotubes. Toxicol Appl Pharmacol 207:221–31.

Murphy FA, Poland CA, Duffin R, et al. 2011. Length-dependent retention of carbon nanotubes in the pleural space of mice initiates sustained inflammation and progressive fibrosis on the parietal pleura. Am J Pathol 178:2587–600.

Murray AR, Kisin ER, Tkach AV, Yanamala N, Mercer R, Young SH, et al. 2012. Factoring-in agglomeration of carbon nanotubes and nanofibers for better prediction of their toxicity versus asbestos. Part Fibre Toxicol 9:10.

Mutlu GM, Budinger GR, Green AA, et al. 2010. Biocompatible nanoscale dispersion of single-walled carbon nanotubes minimizes *in vivo* pulmonary toxicity. Nano Lett 10:1664–70.

O'Brien J, Wilson I, Orton T, Pognan F. 2000. Investigation of the Alamar Blue (resazurin) fluorescent dye for the assessment of mammalian cell cytotoxicity. Eur J Biochem 267:5421–6.

Park EJ, Cho WS, Jeong J, Yi J, Choi K, Park K. 2009. Pro-inflammatory and potential allergic responses resulting from B cell activation in mice treated with multi-walled carbon nanotubes by intratracheal instillation. Toxicology 259:113–21.

Pauluhn J. 2009. Comparative pulmonary response to inhaled nanostructures: considerations on test design and endpoints. Inhal Toxicol 21:40–54.

Pauluhn J. 2010. Subchronic 13-week inhalation exposure of rats to multiwalled carbon nanotubes: toxic effects are determined by density of agglomerate structures, not fibrillar structures. Toxicol Sci 113: 226–42.

Poland CA, Byrne F, Cho WS, et al. 2012. Length-dependent pathogenic effects of nickel nanowires in the lungs and the peritoneal cavity. Nanotoxicology 6:899–911.

Ponti J, Colognato R, Rauscher H, Gioria S, Broggi F, Franchini F, et al. 2010. Colony forming efficiency and microscopy analysis of multi-wall carbon nanotubes cell interaction. Toxicol Lett 197: 29–37.

Porter DW, Hubbs AF, Chen BT, et al. 2013. Acute pulmonary dose-responses to inhaled multi-walled carbon nanotubes. Nanotoxicology 7:1179–94.

Pulskamp K, Diabate S, Krug HF. 2007. Carbon nanotubes show no sign of acute toxicity but induce intracellular reactive oxygen species in dependence on contaminants. Toxicol Lett 168: 58–74.

Ravichandran P, Baluchamy S, Sadanandan B, Gopikrishnan R, Biradar S, Ramesh V, et al. 2010. Multiwalled carbon nanotubes activate NF-kappaB and AP-1 signaling pathways to induce apoptosis in rat lung epithelial cells. Apoptosis 15:1507–16.

Ravichandran P, Periyakaruppan A, Sadanandan B, Ramesh V, Hall JC, Jejelowo O, Ramesh GT. 2009. Induction of apoptosis in rat lung epithelial cells by multiwalled carbon nanotubes. J Biochem Mol Toxicol 23:333–44.

Reddy AR, Reddy YN, Krishna DR, Himabindu V. 2010. Pulmonary toxicity assessment of multiwalled carbon nanotubes in rats following intratracheal instillation. Environ Toxicol 27:211–9.

Roebben G, Rasmussen K, Kestens V, Linsinger TPJ, Rauscher H, Emons H, Stamm H. 2013. Reference materials and representative test materials: the nanotechnology case. J Nanopart Res 15.

Rotoli BM, Bussolati O, Barilli A, Zanello PP, Bianchi MG, Magrini A, et al. 2009. Airway barrier dysfunction induced by exposure to carbon nanotubes *in vitro*: which role for fiber length? Hum Exp Toxicol 28: 361–8.

Rotoli BM, Bussolati O, Bianchi MG, Barilli A, Balasubramanian C, Bellucci S, Bergamaschi E. 2008. Non-functionalized multi-walled carbon nanotubes alter the paracellular permeability of human airway epithelial cells. Toxicol Lett 178:95–102.

Ryman-Rasmussen JP, Tewksbury EW, Moss OR, Cesta MF, Wong BA, Bonner JC. 2009. Inhaled multiwalled carbon nanotubes potentiate airway fibrosis in murine allergic asthma. Am J Respir Cell Mol Biol 40:349–58.

Sakagami M. 2006. *In vivo, in vitro* and *ex vivo* models to assess pulmonary absorption and disposition of inhaled therapeutics for systemic delivery. Adv Drug Deliv Rev 58:1030–60.

Saleh NB, Pfefferle LD, Elimelech M. 2010. Influence of biomacromolecules and humic acid on the aggregation kinetics of single-walled carbon nanotubes. Environ Sci Technol 44:2412–18.

Salem LB, Bosquillon C, Dailey LA, Delattre L, Martin GP, Evrard B, Forbes B. 2009. Sparing methylation of beta-cyclodextrin mitigates cytotoxicity and permeability induction in respiratory epithelial cell layers *in vitro*. J Control Release 136:110–16.

Scholzen T, Gerdes J. 2000. The Ki-67 protein: from the known and the unknown. J Cell Physiol 182:311–22.

Shvedova AA, Kisin ER, Porter D, Schulte P, Kagan VE, Fadeel B, Castranova V. 2009. Mechanisms of pulmonary toxicity and medical applications of carbon nanotubes: two faces of Janus? Pharmacol Ther 121:192–204.

Shvedova AA, Pietroiusti A, Fadeel B, Kagan VE. 2012. Mechanisms of carbon nanotube-induced toxicity: focus on oxidative stress. Toxicol Appl Pharmacol 261:121–33.

Shvedova AA, Tkach AV, Kisin ER, et al. 2013. Carbon nanotubes enhance metastatic growth of lung carcinoma via up-regulation of myeloid-derived suppressor cells. Small 9:1691–5.

Simon-Deckers A, Gouget B, Mayne-L'hermite M, Herlin-Boime N, Reynaud C, Carriere M. 2008. *In vitro* investigation of oxide nanoparticle and carbon nanotube toxicity and intracellular accumulation in A549 human pneumocytes. Toxicology 253: 137–46.

Smart SK, Cassady AI, Lu GQ, Martin DJ. 2006. The biocompatibility of carbon nanotubes. Carbon 44:1034–47.

Teijeiro-Osorio D, Remunan-Lopez C, Alonso MJ. 2009. New generation of hybrid poly/oligosaccharide nanoparticles as carriers for the nasal delivery of macromolecules. Biomacromolecules 10:243–9.

Thubagere A, Reinhard BM. 2010. Nanoparticle-induced apoptosis propagates through hydrogen-peroxide-mediated bystander killing:

insights from a human intestinal epithelium *in vitro* model. ACS Nano 4:3611–22.
Vogel V, Sheetz M. 2006. Local force and geometry sensing regulate cell functions. Nat Rev Mol Cell Biol 7:265–75.
Vogel V, Sheetz MP. 2009. Cell fate regulation by coupling mechanical cycles to biochemical signaling pathways. Curr Opin Cell Biol 21: 38–46.
Wang L, Stueckle TA, Mishra A, Derk R, Meighan T, Castranova V, Rojanasakul Y. 2013. Neoplastic-like transformation effect of single-walled and multi-walled carbon nanotubes compared to asbestos on human lung small airway epithelial cells. Nanotoxicology, in press.
Worle-Knirsch JM, Pulskamp K, Krug HF. 2006. Oops they did it again! Carbon nanotubes hoax scientists in viability assays. Nano Lett 6: 1261–8.

Supplementary material available online

Supplementary figure S1–S4.